

Recovery of Platinum Group Metals from Spent Catalysts Using Iron Chloride Vapor Treatment



YU-KI TANINOUCI and TORU H. OKABE

The recovery of platinum group metals (PGMs) from spent automobile catalysts is a difficult process because of their relatively low contents in the scrap. In this study, to improve the efficiency of the existing recycling techniques, a novel physical concentration method involving treatment with FeCl_2 vapor has been examined. The reactions occurring between typical catalyst components and FeCl_2 vapor are discussed from the thermodynamic point of view, and the validity of the proposed technique was experimentally verified. The obtained results indicate that the vapor treatment at around 1200 K (927 °C) can effectively alloy PGMs (Pt, Pd, and Rh) with Fe, resulting in the formation of a ferromagnetic alloy. It was also confirmed that cordierite and alumina (the major catalyst components) remained unreacted after the vapor treatment, while ceria species were converted into oxychlorides. The samples simulating the automobile catalyst were also subjected to magnetic separation after the treatment with FeCl_2 vapor; as a result, PGMs were successfully extracted and concentrated in the form of a magnetic powder. Thus, the FeCl_2 vapor treatment followed by magnetic separation can be utilized for recovering PGMs directly from spent catalysts as an effective pretreatment for the currently used recycling methods.

<https://doi.org/10.1007/s11663-018-1269-9>

© The Minerals, Metals & Materials Society and ASM International 2018

I. INTRODUCTION

PLATINUM group metals (PGMs) are expensive and relatively scarce elements in the Earth's crust. The mineral resources of PGMs are predominately localized in South Africa and Russia.^[1–4] Furthermore, their extraction and subsequent treatment generate large amounts of waste and consume a lot of energy. PGMs are widely used in various industrial applications because of their unique catalytic properties and excellent heat and corrosion resistances. In particular, automobile catalysts account for a large fraction of the global demand for Pt, Pd, and Rh.^[1] Therefore, the recovery of PGMs from spent automobile catalysts is important not only in terms of ensuring their steady supply, but also minimizing the environmental burden.

The recycling of PGMs from spent catalysts has been actively practiced by many smelting and recycling companies. However, the efficient recovery of these metals is difficult because of their relatively low concentrations in the scrap and high chemical stability.

Automobile catalysts mostly consist of honeycomb-structured ceramic substrates with porous catalyst layer. The ceramic substrates are composed of cordierite ($\text{Mg}_2\text{Al}_4\text{Si}_5\text{O}_{18}$) or similar chemically stable oxides. The catalyst layers that support fine PGM particles consist of alumina (Al_2O_3) and other oxides such as ceria (CeO_2) and zirconia (ZrO_2). The total concentration of PGMs in the catalysts is approximately 0.05–0.5 mass pct (500–5000 ppm).^[5]

Usually, the catalysts recovered from used automobiles are first mechanically pulverized to evaluate their PGM contents and then subjected to pyrometallurgical and/or hydrometallurgical processes for PGM extraction (see Figure 1).^[2–5] In commercial applications, pulverized catalysts are often smelted with a collector metal such as liquid Fe or Cu; hereby, PGMs are concentrated in the metallic phase, while the ceramic components of the spent catalysts are removed as slag waste.^[6,7] Subsequently, the PGMs extracted in the collector metal are dissolved in an aqueous solution followed by their separation and purification using various techniques such as solvent extraction, precipitation, and ion exchange.^[8,9] The benefits of the pyrometallurgical processing method include large PGM recovery rates and high throughput. However, its practical implementation requires the use of large-scale equipment and high amount of energy. It should also be noted that PGMs could be dissolved directly from spent catalysts in strong oxidizing acids, such as

YU-KI TANINOUCI and TORU H. OKABE are with the Institute of Industrial Science, The University of Tokyo, 4-6-1 Komaba, Meguro-ku, Tokyo 153-8505, Japan. Contact e-mail: taninou@iis.u-tokyo.ac.jp

Manuscript submitted December 18, 2017.

Article published online May 7, 2018.

aqua regia and hydrochloric acid with chlorine gas, which is typically performed using a small-scale plant with relatively low energy consumption. However, the applicability of this method is often limited by the low PGM recovery rates, longer processing times, and generation of large volumes of toxic waste solutions and gases.

A physical separation pretreatment aimed at concentrating PGMs directly from spent catalysts can potentially improve the efficiency and throughput of the existing recycling processes. To achieve this goal, various techniques such as magnetic separation,^[10,11] flotation,^[11,12] selective grinding followed by size separation,^[13,14] selective grinding after a heating/quenching treatment,^[15] and physical separation methods involving simple chemical pretreatments such as alloying, sulfurization, and plating^[16–20] have been proposed and studied. However, these techniques are either in the developmental stage or not practically feasible for the industrial use.

The objective of this study is to investigate the feasibility and industrial applicability of the novel physical concentration process illustrated in Figure 1. The proposed method involves a chemical pretreatment stage and uses the concept outlined in the patent

invented by Okabe and Mitsui.^[16] For effectively concentrating PGMs *via* magnetic separation, they are converted into ferromagnetic Fe-PGM alloys through the reaction with FeCl_2 vapor. It is also notable that the dissolution of PGMs can be promoted by alloying with less noble metals^[2,21,22]; thus, alloying with Fe would be useful not only for magnetically separating PGMs, but also for facilitating their dissolution in acid.

In a previous study, we examined possible reactions between pure Pt and FeCl_x ($x = 2, 3$).^[20] It was found that Pt metal could be effectively converted into a ferromagnetic alloy through its reaction with FeCl_2 in the presence of metallic Fe, and the corresponding alloying reaction was represented by the disproportionation of FeCl_2 vapor. The modern automobile catalysts also contain other PGMs such as Pd and Rh, while their major components consist of various oxides (such as cordierite and Al_2O_3). Therefore, in this study, to further investigate the proposed route, the reactivities of these compounds during the FeCl_2 vapor treatment were examined theoretically and experimentally. Moreover, the magnetic concentration of PGMs was demonstrated using the samples simulating an automobile catalyst.

II. TREATMENT WITH IRON CHLORIDE VAPOR

A. Theoretical Background

Figure 2 outlines the proposed FeCl_2 vapor treatment procedure. The volatilities of FeCl_x species are sufficiently high; in particular, the vapor pressures of FeCl_2 and FeCl_3 exceed 10^{-1} atm at temperatures above 1090 K and 540 K (817 °C and 267 °C), respectively.^[23] Thus, FeCl_2 vapor can be effectively supplied to the PGMs located on the complex porous surfaces of catalysts by heating its source. The utilized reaction system is loaded with metallic Fe characterized by high affinity to PGMs (the treatment chamber either is fabricated from steel or contains pieces of metallic Fe). As a result, under suitable conditions, the gaseous phase acts as a medium that transports Fe from the metallic

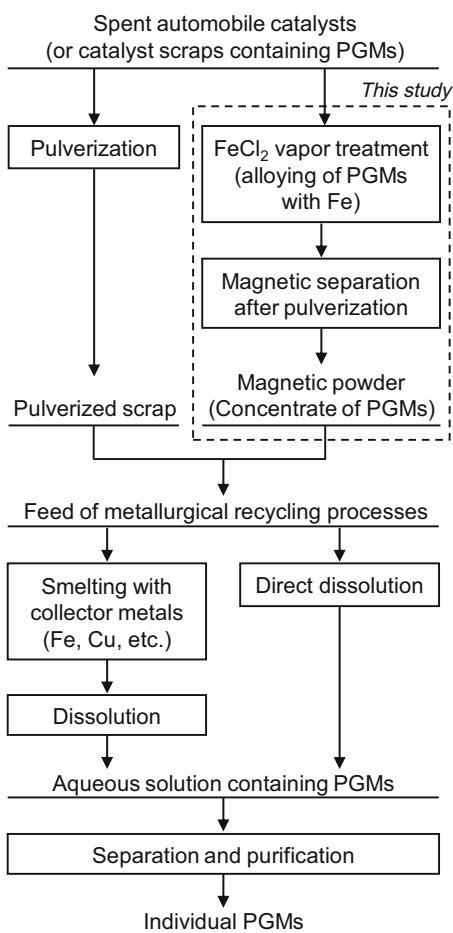


Fig. 1—Diagram describing the novel physical concentration method proposed in this study and common procedure for recovering PGMs from spent catalysts.

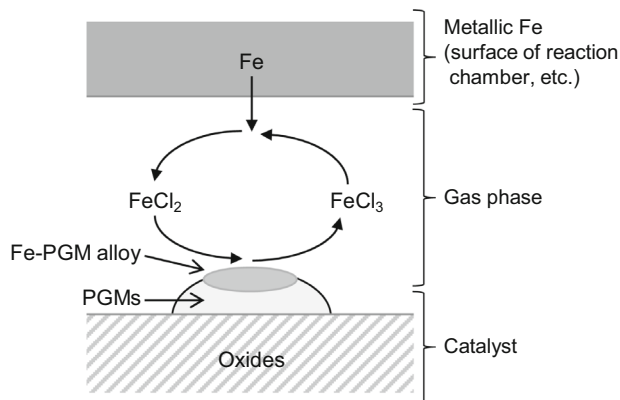
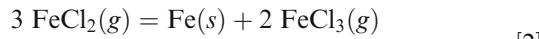


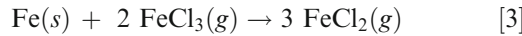
Fig. 2—Schematic illustration of the FeCl_2 vapor treatment procedure. The PGMs in spent catalysts are alloyed with Fe through the disproportionation of FeCl_2 vapor.

phase to the PGMs, and alloys them together *via* the following disproportionation reaction^[20]:



$$\Delta G_{(2)}^\circ = 126 \text{ kJ at } 1200 \text{ K (927 } ^\circ\text{C)},^{[23]}$$

where $\Delta G_{(2)}^\circ$ denotes the standard Gibbs energy change of reaction [2]. The FeCl_3 molecules generated by the disproportionation reaction diffuse into the gas phase and then react with metallic Fe to regenerate FeCl_2 .



The overall reaction can be expressed as follows:



After the vapor treatment, FeCl_x species may attach to the scrap surface. However, they can be further separated and recovered from the scrap *via* evaporation without producing a toxic waste solution. If all PGMs are alloyed through the described mechanism while the ceramic components remain unreacted, the supplied FeCl_2 species can be conserved and recycled for the subsequent use.

B. Thermodynamic Considerations

In this section, the reactions occurring during the FeCl_2 vapor treatment are further examined at a temperature of 1200 K (927 °C), which was effectively used for alloying Pt samples with Fe in a previous study.^[20] At this temperature, FeCl_2 is a liquid, and its vapor pressure can be as high as 3.2×10^{-1} atm.^[23]

In Figure 3, the chemical potentials of chlorine (p_{Cl_2}) corresponding to the Pt/PtCl₂, Pd/PdCl₂, and Rh/RhCl₃ equilibria are listed on the potential diagram of the Fe-Cl system. The thermodynamic data provided in Reference 23 were used during calculations. At around 1200 K (927 °C), the p_{Cl_2} corresponding to the equilibrium between PGMs and their chlorides is significantly higher than the values obtained at the Fe/FeCl₂ and FeCl₂/FeCl₃ equilibria. Thus, it can be assumed that Pt, Pd, and Rh are not chlorinated during the FeCl_2 vapor treatment.

Figure 4 shows the phase diagrams of the Fe-Pt, Fe-Pd, and Fe-Rh systems.^[24,25] The α -phase, which is a solid solution with a body-centered cubic structure, exhibits ferromagnetic properties at ambient temperature (around 298 K). Furthermore, the γ_1 -Fe₃Pt and γ_2 -FePt phases of the Fe-Pt system, γ_1 -FePd and γ_2 -FePd₃ phases of the Fe-Pd system, and α' -(Fe,Rh) phase of the Fe-Rh system can be also ferromagnetic at such a temperature. To achieve efficient recovery of PGMs from the catalyst scrap by magnetic separation, they should be converted into these ferromagnetic alloys through vapor treatment. For example, if the Fe concentration in Pd exceeds approximately 15 mol pct

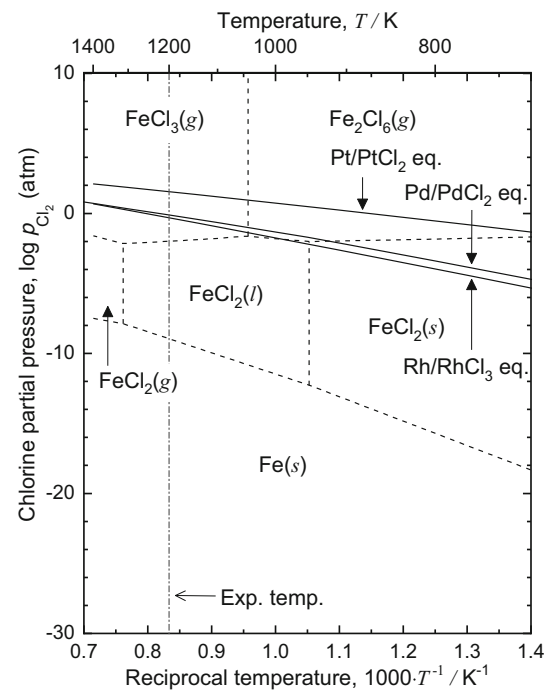


Fig. 3—Chemical potentials of chlorine corresponding to the equilibria between PGMs and their chlorides as functions of temperature. The chemical potential diagram of the Fe-Cl system is plotted as the dotted line. The thermodynamic data reported in Ref. [23] were used.

after performing reaction [1] at 1200 K (927 °C), ferromagnetic Fe-Pd alloys (α -(Fe,Pd), γ_1 -FePd, and/or γ_2 -FePd₃) can be formed during cooling or by annealing at intermediate temperatures. To obtain ferromagnetic Fe-Rh alloys at ambient temperature (such as α -(Fe,Rh) and/or α' -(Fe,Rh)), the Fe concentration in Rh should be increased above approximately 40 mol pct.

From the viewpoint of equilibrium, the alloying of PGMs proceeds until the activity of Fe (a_{Fe}) in the Fe-PGM alloy becomes equal to the a_{Fe} of the reaction system. Since the utilized reaction system contains excess amounts of metallic Fe, its a_{Fe} is almost unity. Thus, the proposed vapor treatment can potentially increase the Fe concentration in PGMs to an amount sufficient for the formation of ferromagnetic alloys. In order to consider the reaction rate of PGM alloying, the relationship between a_{Fe} and the equilibrium partial pressure of FeCl_3 (p_{FeCl_3}) under the specified p_{FeCl_2} was calculated at 1200 K (927 °C) using the thermodynamic data reported in Reference 23. The result is shown in Figure 5. The equilibrium p_{FeCl_3} decreases with an increase in a_{Fe} (or with alloying Fe). When the p_{FeCl_2} is 3.2×10^{-1} atm (corresponding to the saturated vapor pressure of FeCl_2), the equilibrium p_{FeCl_3} of the produced Fe-PGM alloy is higher than 3×10^{-4} atm and can be as high as 1×10^{-3} atm at $a_{\text{Fe}} = 1 \times 10^{-1}$ (where γ_2 -FePt phase is stable in the Fe-Pt system^[26]). Thus, the reaction of FeCl_2 vapor with PGMs can proceed relatively fast.

In general, the cordierite and Al_2O_3 phases are the major components of honeycomb-structured substrate and porous catalyst layer, respectively. In order to

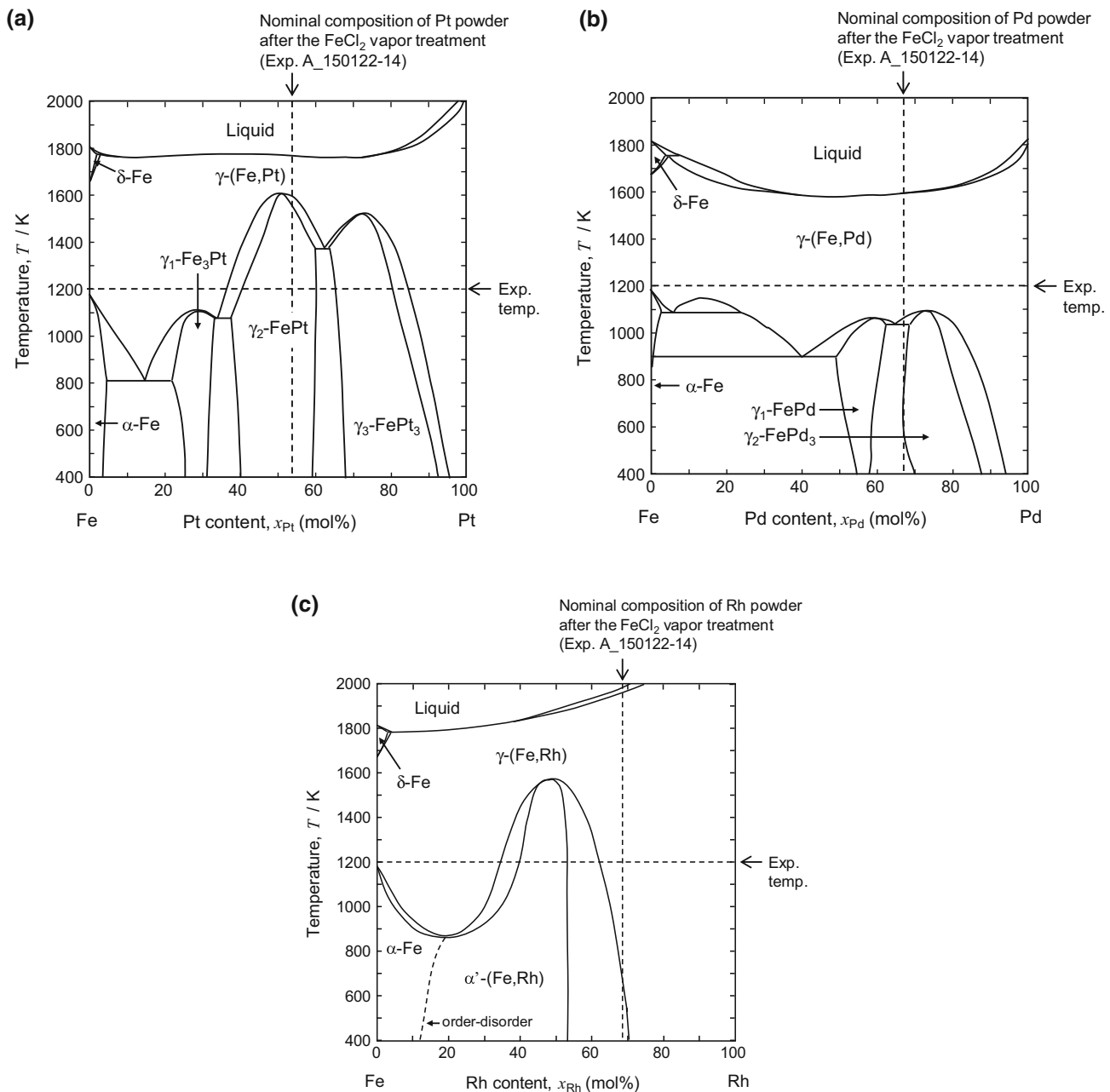


Fig. 4—Phase diagrams of the (a) Fe-Pt, (b) Fe-Pd, and (c) Fe-Rh systems adapted from Refs. [24] and [25]. The phases denoted by γ_i correspond to fcc-based ordered structures.

analyze the reactivities of these oxides during the FeCl_2 vapor treatment, chemical potential diagrams of the M-Cl-O system (M: Al, Mg, Si, and Fe) were constructed at 1200 K (927 °C) using the thermodynamic data reported in the literature.^[23]

Figure 6(a) is constructed by overlapping the chemical potential diagram of the Al-Cl-O system with that of the Fe-Cl-O system. The diagram is described using the logarithms of the partial pressure of chlorine (p_{Cl_2}) and partial pressure of oxygen (p_{O_2}) as the abscissa and ordinate, respectively. During the vapor treatment, sufficient amounts of Fe and FeCl_2 are present in the reaction system, and the magnitude of p_{FeCl_2}

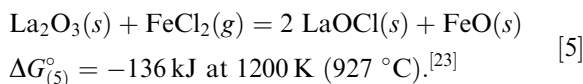
corresponds to the saturated vapor pressure of liquid FeCl_2 . In this case, the p_{Cl_2} and p_{O_2} of the reaction system can be determined by the Fe/ FeCl_2 and Fe/ FeO equilibria, respectively. Therefore, the chemical potential of the reaction system is located near the potential point α in the figure. At this chemical potential, the Al_2O_3 phase is thermodynamically stable, which indicates that Al_2O_3 species present in the catalyst scrap likely remain unreacted during the vapor treatment.

In Figure 6(b), the chemical potential diagram of the Mg-O-Cl system is overlaid on that of the Fe-O-Cl system. Meanwhile, in Figure 6(c), the chemical potential diagram of the Si-O-Cl system is overlaid on that of

the Fe-O-Cl system. At the potential point α , both the MgO and SiO₂ phases are stable. Since cordierite is a complex oxide of Al₂O₃, MgO, and SiO₂, it is expected not to react with FeCl₂ vapor.

The reactivities of ZrO₂, La₂O₃, and CeO₂ species are also analyzed, because these oxides and/or their solid solutions are often contained in the porous catalyst layer of automobile catalysts. The chemical potential diagrams shown in Figure 7 were constructed at 1200 K (927 °C) using the thermodynamic data reported in the literature.^[23] The standard Gibbs energy of formation of CeOCl was estimated from its standard enthalpy of formation at 298 K (25 °C)^[27] and the Gibbs energy function of the formation of LaOCl^[23] (the details of the utilized procedure are provided elsewhere^[28]).

As shown in Figure 7(a), the ZrO₂ phase is stable near the potential point α corresponding to the chemical potential at the Fe/FeCl₂/FeO equilibrium. Thus, ZrO₂ species in the catalyst scrap are expected to remain unreacted during the vapor treatment. Meanwhile, the La₂O₃ and CeO₂ phases are unstable at the potential point α , as shown in Figures 7(b) and (c), respectively. Because LaOCl is stable at the potential point α , the La₂O₃ species contained in the scrap are expected to react with FeCl₂ vapor as follows:



For the CeO₂ species, the following reaction is expected to occur:

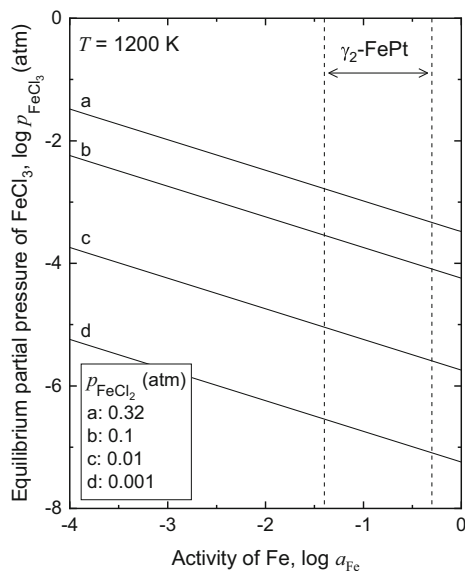
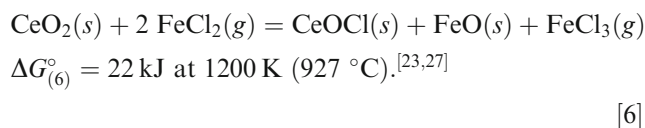
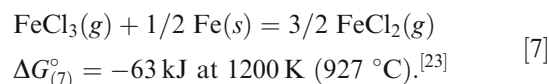
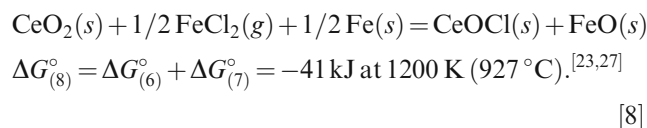


Fig. 5—Partial pressure of FeCl₃ equilibrated with Fe-PGM alloy at the specified partial pressures of FeCl₂ and temperature of 1200 K (927 °C). The thermodynamic data reported in Ref. [23] were used. The saturated vapor pressure of FeCl₂ at 1200 K (927 °C) is 0.32 atm.

The gaseous FeCl₃ generated by reaction [6] will react with metallic Fe in the reaction system.



Thus, the overall reaction can be expressed as follows:



III. MATERIALS AND METHODS

A. Sample Preparation

Table I lists all the samples used in this study. Powders of PGMs (Pt, Pd, and Rh), cordierite, Al₂O₃, ZrO₂, La₂O₃, and CeO₂ were used as the starting materials during the FeCl₂ vapor treatment. Furthermore, plate-type catalyst samples were prepared to simulate the automobile catalyst. Since the procedure for the preparation of the catalyst sample has been previously described in detail elsewhere,^[17] only a brief outline is provided in this study. First, Pt-, Pd-, and Rh-loaded alumina powders were synthesized by baking γ -Al₂O₃ powder impregnated with aqueous solutions of various PGMs and then mixed with boehmite powder and diluted aqueous solution of HNO₃ to prepare slurry. The latter was coated onto an Al₂O₃ plate with an area of approximately 25 × 25 mm² and thickness of 0.5 mm and then baked at 1073 K (800 °C) for 3 hours in vacuum. The thickness of the porous catalyst layer formed on the Al₂O₃ plate was several hundred micrometers (see Figure 15(a)), and the concentration of each PGM in the catalyst samples was approximately 0.04 mass pct (see Table III).

B. Experimental Procedure

The experimental apparatus used for the FeCl₂ vapor treatment is shown in Figure 8, while the masses of the feed materials are listed in Table II. The tested samples were held in a quartz crucibles, which were subsequently placed in the reaction chamber fabricated from mild steel, as shown in Figures 8(a) and (b). A mixture of Fe powder (> 95 pct; Wako Pure Chemical Industries, Ltd.) and FeCl₂ powder (99.9 pct; Wako Pure Chemical Industries, Ltd.) was placed at the chamber's bottom. To prevent the water adsorption by FeCl₂, the mixture of Fe and FeCl₂ was prepared inside a glove box under a high-purity N₂ atmosphere. The reaction chamber was covered with a steel cap without sealing. As shown in Figure 8(c), the reaction chamber was positioned at the bottom of a vertical gas-tight quartz tube. The interior of this tube was evacuated using a rotary pump, following which the exhaust port located at the tube top was closed.

To perform the vapor treatment procedure at 1200 K (927 °C), the quartz tube containing the reaction

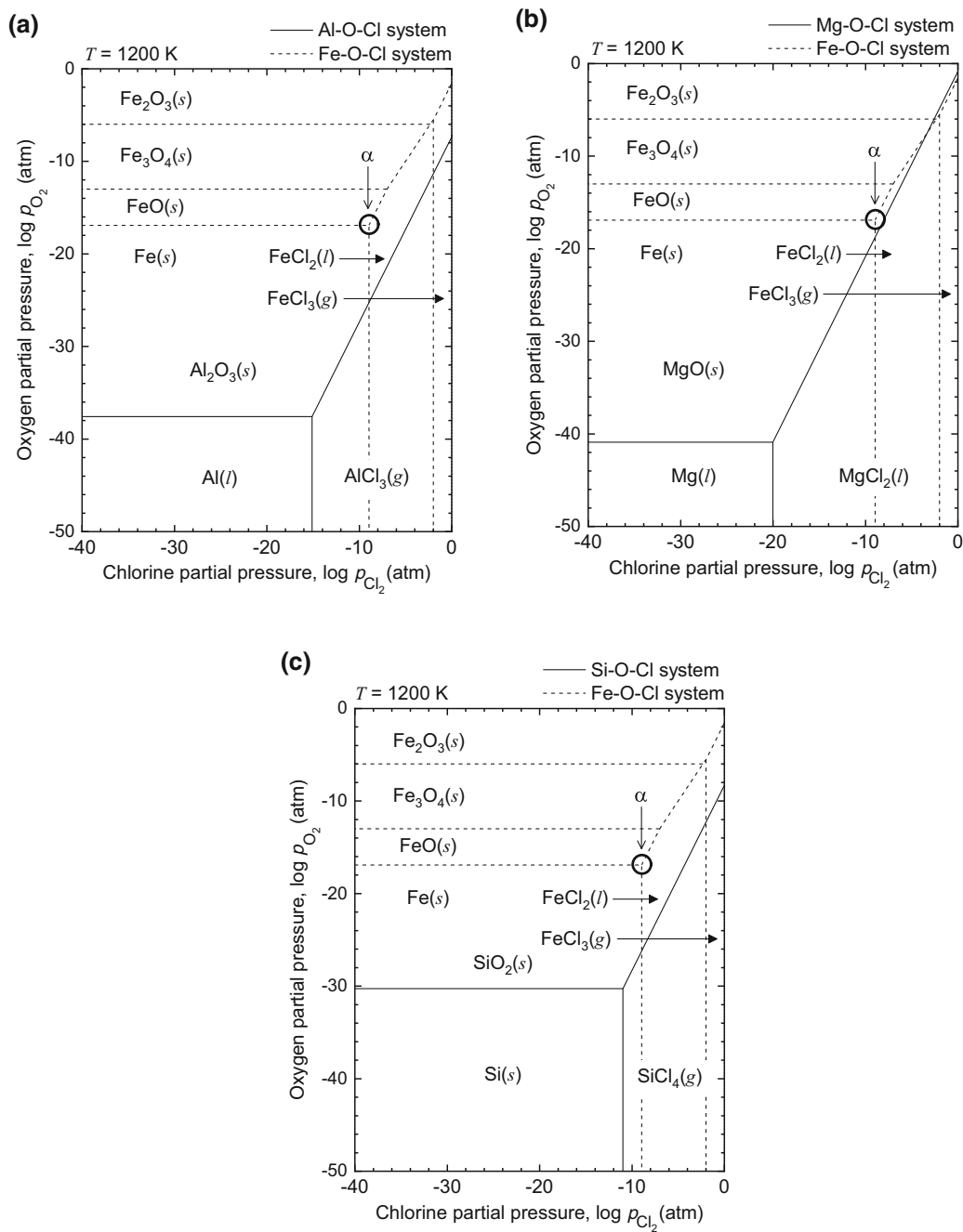


Fig. 6—Combined chemical potential diagrams of the (a) Al-O-Cl and Fe-O-Cl, (b) Mg-O-Cl and Fe-O-Cl, and (c) Si-O-Cl and Fe-O-Cl systems constructed at 1200 K (927 °C). The thermodynamic data reported in Ref. [23] were used. The potential point α corresponds to the Fe/FeCl₂/FeO equilibrium.

chamber was introduced into a preheated vertical furnace and kept there for 1.5 hours. Afterward, the quartz tube was removed from the furnace and cooled in air. Figure 9 shows the temperature profile recorded inside the quartz tube. The temperature measured at the location of the reaction chamber reached 1200 K (927 °C) after 0.5 hour and then was maintained at that level for 1 hour, as shown in Figure 9(a). During the heat treatment, the upper part of the quartz tube was kept at a lower temperature, as shown in Figure 9(b).

After the heat treatment, Ar gas or air was introduced inside the quartz tube to reach atmospheric pressure, and then the rubber plug was removed from the top of the tube. Subsequently, the samples in the reaction chamber and deposits accumulated on the inner wall of the quartz tube were recovered. The crystalline phases of the processed powder samples and deposits on the tube wall were analyzed by X-ray diffraction (XRD) using a D2 PHASER (Bruker Corporation, Cu-K α radiation). In some experiments, qualitative elemental analysis was

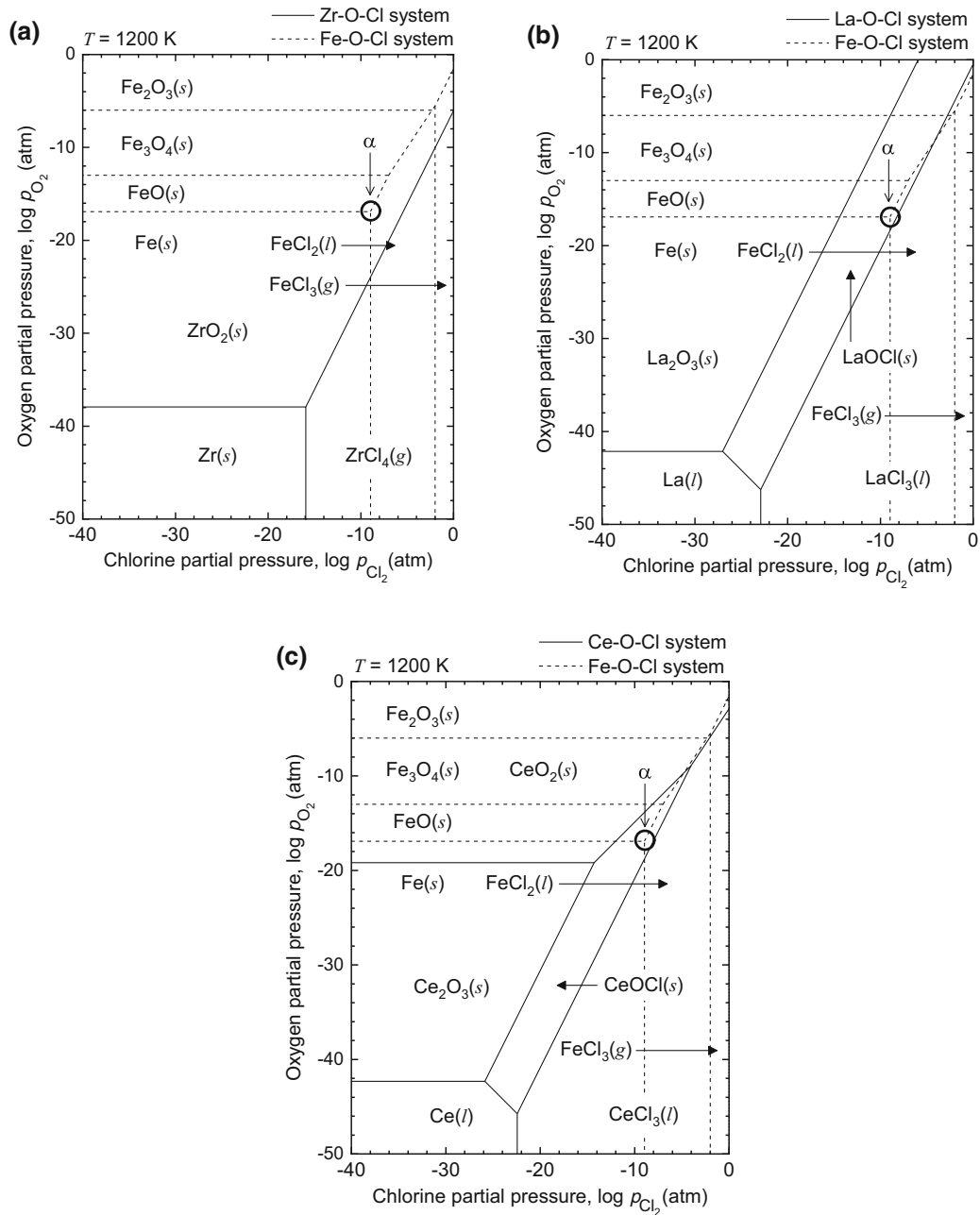


Fig. 7—Combined chemical potential diagrams of the (a) Zr-O-Cl and Fe-O-Cl, (b) La-O-Cl and Fe-O-Cl, and (c) Ce-O-Cl and Fe-O-Cl systems constructed at 1200 K (927 °C). The thermodynamic data reported in Refs. [23] and [27] were used. The potential point α corresponds to the Fe/FeCl₂/FeO equilibrium.

performed by X-ray fluorescence spectroscopy (XRF) using a JSX-3100R11 (JEOL).

When the tested sample was a plate-type simulated catalyst, it was manually crushed and pulverized using an agate mortar after the treatment with FeCl₂ vapor. Subsequently, magnetic separation was performed by hand using a handheld neodymium magnet (Nd-Fe-B alloy; diameter: 30 mm, thickness: 15 mm, surface magnetic flux density: 490 mT). The PGM concentrations in the obtained magnetic and nonmagnetic powders were determined by inductively coupled plasma-atomic emission spectrometry (ICP-AES) using

an SPS3520UV (SII NanoTechnology). The procedure for preparing sample solutions for ICP-AES is described in detail elsewhere.^[17] In this study, the PGM concentration in the catalyst sample before processing ($C_{cat,i}$ (mass pct), i : Pt, Pd, or Rh) was evaluated based on the masses and PGM concentrations in the magnetic and nonmagnetic powders as follows:

$$C_{cat,i} = (C_{mag,i} \times w_{mag} + C_{nmag,i} \times w_{nmag}) / w_{cat} \quad [9]$$

Here $C_{mag,i}$ and $C_{nmag,i}$ are the PGM concentrations in the magnetic and nonmagnetic powders determined by ICP-AES, respectively; w_{mag} and w_{nmag} are the masses

Table I. Samples Used in This Study

Material	Form	Purity or Conc. (Mass pct)	Note
Pt	Powder	99.95	Supplied by Tanaka Kikinzoku Kogyo K.K. Micrometer sized, gray color.
Pd	Powder	> 99.98	Supplied by Furuya Metal Co., Ltd. Micrometer sized, gray color.
Rh	Powder	> 99.9	Supplied by Tanaka Kikinzoku Kogyo K.K. Micrometer sized, gray color.
Cordierite	Powder	> 95	Supplied by Marusu Glaze Co., Ltd. Product name: SS-200.
Al ₂ O ₃	Powder	> 99.5	Supplied by Wako Pure Chemical Industries, Ltd. Alfa alumina.
ZrO ₂	Powder	99.9	Supplied by Kanto Chemical Co., Inc.
La ₂ O ₃	Powder	> 98	Supplied by Wako Pure Chemical Industries, Ltd.
CeO ₂	Powder	> 99.5	Supplied by Kanto Chemical Co., Inc.
Simulated catalyst	Plate	Pt ~ 0.04 Pd ~ 0.04 Rh ~ 0.04	Self-prepared sample. A PGM-bearing catalyst layer was formed on an alumina plate with dimension of approximately 25 × 25 × 0.5 mm.

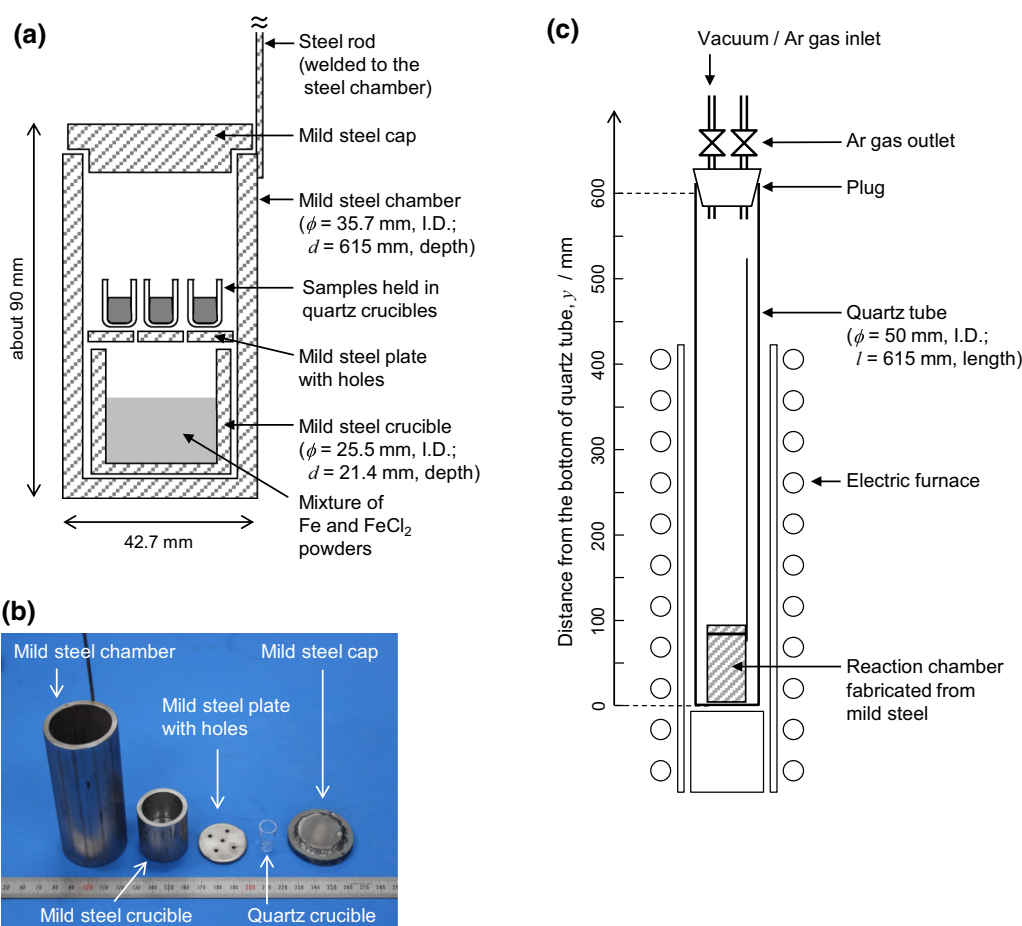


Fig. 8—(a) Schematic illustration of the reaction chamber and (b) a photograph of its parts before assembly. (c) Schematic illustration of the experimental apparatus used for the FeCl₂ vapor treatment.

of the magnetic and nonmagnetic powders, respectively; and w_{cat} is the mass of the catalyst sample before experiment. Furthermore, in order to evaluate

the efficiency of the magnetic separation, the enrichment factor (F_i) and recovery rate (R_i (pct)) of the PGMs were calculated as follows:

Table II. Experimental Conditions of the FeCl₂ Vapor Treatment and the Corresponding Weight Changes of the Studied Samples

Exp. No.	Mass of Fe, w_{Fe}/g	Mass of FeCl ₂ , w_{FeCl_2}/g	Processed Sample	Experimental Results		
				Mass of the Sample Before Vapor Treatment, $w_{s,before}/g$	Mass of the Sample After Vapor Treatment, $w_{s,after}/g$	Weight Change, X (pct) ^d
A_150122-14 ^a	1.022	2.936	Pt powder	0.3997	0.4959	24
			Pd powder	0.3759	0.4749	26
			Rh powder	0.3844	0.4761	24
B_150119-10 ^b	1.084	3.053	Cordierite powder	0.2837	0.2909	2.5
			Al ₂ O ₃ powder	0.3139	0.3142	0.1
C_150122-15 ^b	1.001	3.031	ZrO ₂ powder	0.3990	0.4149	4.0
			La ₂ O ₃ powder	0.4118	0.6336	54
			CeO ₂ powder	0.4129	0.5583	35
D_150629-16 ^c	1.040	2.996	Simulated catalyst	1.434	1.453	1.4
E_151024-18 ^c	1.025	5.996	Simulated catalyst	1.450	1.478	1.9

^aEach sample was held in a quartz crucible ($\phi = 12$ mm, I.D.; $d = 20$ mm, depth).

^bEach sample was held in a quartz crucible ($\phi = 9.6$ mm, I.D.; $d = 15$ mm, depth).

^cCatalyst sample was held in a quartz crucible ($\phi = 31$ mm, I.D.; $d = 12$ mm, depth).

^d $X = 100 \times (w_{s,after} - w_{s,before}) / w_{s,before}$.

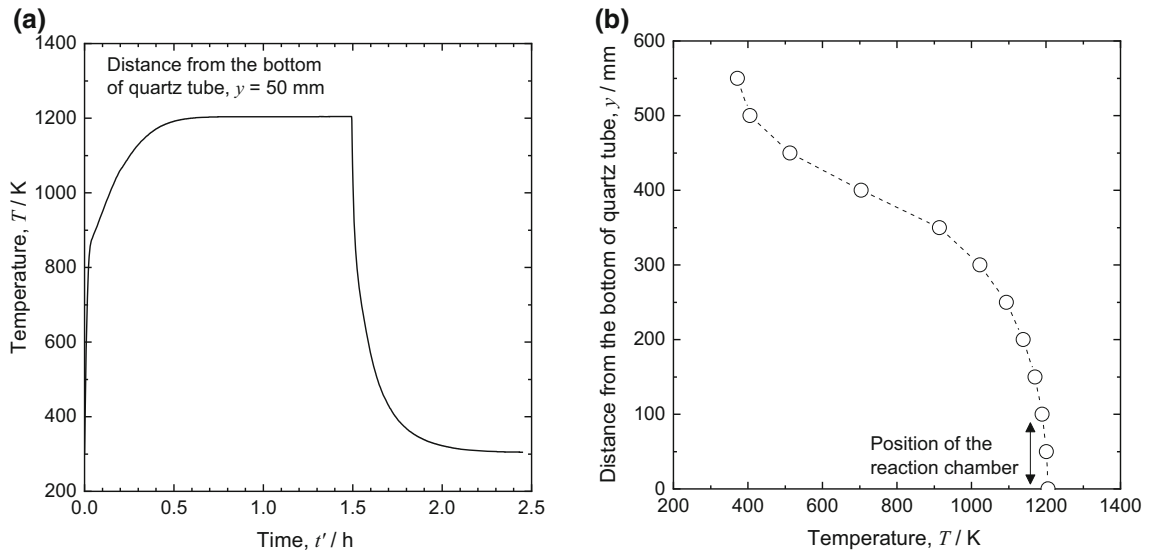


Fig. 9—Temperature profile inside the quartz tube during the FeCl₂ vapor treatment. (a) Temperature change at the position of the steel reaction chamber. (b) Temperature distribution inside the quartz tube when heating the reaction chamber at 1200 K (927 °C).

$$F_i = C_{mag,i} / C_{cat,i} \quad [10]$$

$$R_i = 100 \times (C_{mag,i} \times w_{mag}) / ((C_{mag,i} \times w_{mag}) + (C_{nmag,i} \times w_{nmag})) \quad [11]$$

IV. RESULTS AND DISCUSSION

Figure 10 shows the quartz tube with the steel reaction chamber before and after the FeCl₂ vapor

treatment. After the heat treatment, FeCl₂ disappeared from the chamber bottom, and white deposits identified as FeCl₂ by XRD analysis were formed in the upper part of the quartz tube. This indicates that FeCl₂ vapor was generated in the reaction chamber and diffused upward according to the temperature gradient inside the tube. Based on the visual observation of the upper part of the quartz tube during the heat treatment, the vaporization of FeCl₂ was completed in approximately 1 hour from the start of the heat treatment procedure.

When PGM powders were treated with FeCl₂ vapor, not only Pt, but also Pd and Rh particles were effectively alloyed with Fe. All PGM samples exhibited

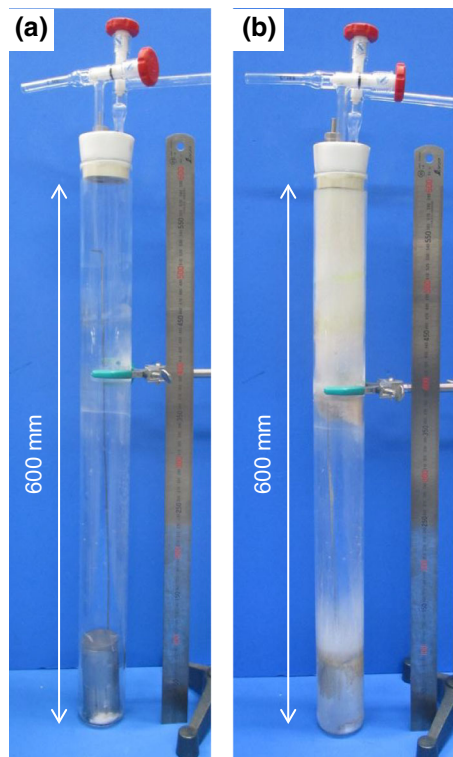


Fig. 10—A quartz tube with the steel reaction chamber (a) before and (b) after the FeCl_2 vapor treatment (Exp. D_150629-16).

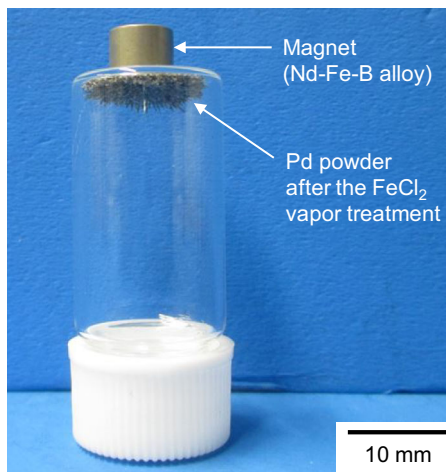


Fig. 11—A photograph of Pd powder obtained after the FeCl_2 vapor treatment (Exp. A_150122-14).

ferromagnetic properties (Figure 11), and their masses increased by approximately 25 pct (Table II). Based on the weight increases, the obtained average compositions of Pt, Pd, and Rh powders after the vapor treatment were $\text{Fe}_{0.46}\text{Pt}_{0.54}$, $\text{Fe}_{0.33}\text{Pd}_{0.67}$, and $\text{Fe}_{0.31}\text{Rh}_{0.69}$, respectively (refer to the phase diagrams in Figure 4). The results of XRD analysis are shown in Figure 12, which suggest that Pt species were converted into the $\gamma_2\text{-FePt}$ ferromagnetic phase. In the Pd sample, the $\gamma_2\text{-FePd}_3$ ferromagnetic phase was formed after the vapor treatment. This means that Pd species were alloyed during

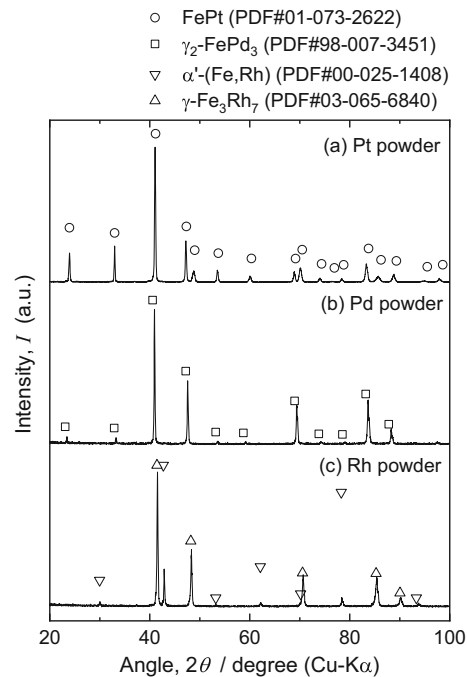


Fig. 12—XRD patterns of (a) Pt, (b) Pd, and (c) Rh powders recorded after the FeCl_2 vapor treatment (Exp. A_150122-14).

the vapor treatment and that the transformation of $\gamma\text{-(Fe,Pd)}$ (disordered face-centered cubic structure) to $\gamma_2\text{-FePd}_3$ (ordered L1_2 structure) proceeded during cooling. The major phase of the Rh sample was the nonmagnetic $\gamma\text{-(Fe,Rh)}$; however, the $\alpha'\text{-(Fe,Rh)}$ ferromagnetic phase was formed as well. This suggests that particles consisting of two phases of $\gamma\text{-(Fe,Rh)}$ and $\alpha'\text{-(Fe,Rh)}$ were formed by the vapor treatment. Prolonged treatment should lead to increased alloying with Fe and an increase in the formation of ferromagnetic phases such as $\alpha'\text{-(Fe,Rh)}$.

Figure 13 shows the XRD patterns of cordierite, Al_2O_3 , and ZrO_2 powders recorded after the vapor treatment. XRD analyses indicated that these oxides remained unreacted, which was consistent with the thermodynamic considerations presented in Section II. The weights of cordierite and ZrO_2 powders slightly increased after the treatment (see Table II), which might be attributed to the addition of a small amount of FeCl_2 into the samples during their recovery from the reaction chamber after the heat treatment.

Figure 14 shows the XRD patterns of La_2O_3 and CeO_2 powders after the vapor treatment. It is clear that both samples reacted with FeCl_2 vapor to form oxychlorides, as was predicted by the thermodynamic analysis presented in Section II. When La_2O_3 and CeO_2 are reacted according to reactions [5] and [6], respectively, FeO is formed as a byproduct. However, its presence was not detected by XRD in this study. The qualitative XRF analysis indicated that La_2O_3 and CeO_2 powders contained Fe species after the vapor treatment. Therefore, it can be concluded that either the amorphous-like FeO phase or another phase was formed during the vapor treatment. According to reactions [5] and [6], the theoretical weight increases of La_2O_3 and

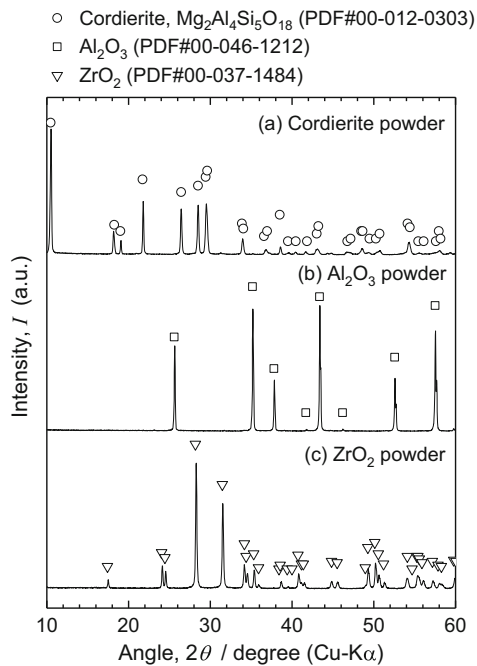


Fig. 13—XRD patterns of (a) cordierite, (b) Al_2O_3 , and (c) ZrO_2 powders recorded after the $FeCl_2$ vapor treatment (Exp. B_150119-10 and C_150122-15).

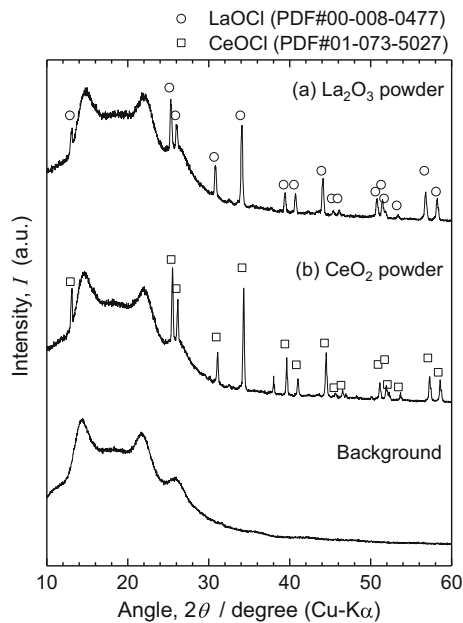


Fig. 14—XRD patterns of (a) La_2O_3 and (b) CeO_2 powders recorded after the $FeCl_2$ vapor treatment (Exp. C_150122-15). The observed background profile originated from the polyimide film, which was used to cover the sample to prevent moisture absorption during measurements.

CeO_2 powders are 61 and 53 pct, respectively. However, the experimental weight gains of these powders determined in this study were 54 and 35 pct, respectively (see Table II). This suggests that parts of the treated samples remained unreacted and/or changed into reaction intermediates because of the relatively short reaction time.

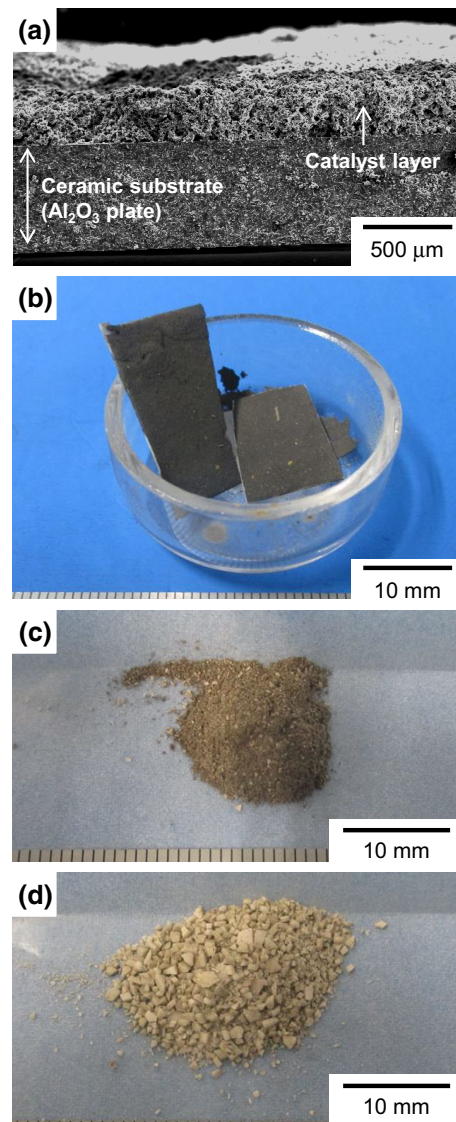


Fig. 15—(a) A cross-sectional SEM image of the catalyst sample reprinted with permission from a previous report Ref. [17]. Photographs of the (b) catalyst sample after the vapor treatment and the (c) magnetic and (d) nonmagnetic powders recovered by magnetic separation (Exp. D_150629-16).

After the $FeCl_2$ vapor treatment followed by pulverization, the catalyst samples were successfully separated into the magnetic and nonmagnetic powders, as shown in Figure 15. This indicates that the present PGM particles were effectively and selectively alloyed with Fe. Table III lists the masses and compositions of these samples, while Table IV provides the corresponding enrichment factors and recovery rates of PGMs. The obtained results show that PGMs were successfully extracted from the catalysts samples and concentrated in the magnetic powder. The magnetic separation procedure increased the concentrations of Pt, Pd, and Rh by a factor of 3 to 5, and the amounts of PGMs in the remaining nonmagnetic powders were negligible. The enrichment factor of PGMs achieved in this study was too low to be used in practical industrial applications.

Table III. Masses and Compositions of the Simulated Catalysts Before and After Processing

Exp. No.	Catalyst Sample			Magnetic Powder			Nonmagnetic Powder					
	Mass, w_{cat}/g	Conc. of Element i , $C_{\text{cat},i}$ (Mass pct) ^a			Mass, w_{mag}/g	Conc. of Element i , $C_{\text{mag},i}$ (Mass pct) ^b			Mass, w_{nmag}/g	Conc. of Element i , $C_{\text{nmag},i}$ (Mass pct) ^b		
		Pt	Pd	Rh		Pt	Pd	Rh		Pt	Pd	Rh
D_150629-16	1.434	0.041	0.039	0.041	0.449	0.13	0.12	0.13	0.993	N.D.	0.002	N.D.
E_151024-18	1.450	0.043	0.041	0.042	0.306	0.20	0.19	0.20	1.152	0.001	0.001	N.D.

N.D.: Practically not detected (< 0.001 mass pct).
^a $C_{\text{cat},i} = (C_{\text{mag},i} \times w_{\text{mag}} + C_{\text{nmag},i} \times w_{\text{nmag}}) / w_{\text{cat}}$.
^bDetermined by ICP-AES.

Table IV. Enrichment Factors and Recovery Rates of PGMs from the Simulated Catalyst Samples

Exp. No.	Enrichment Factor of Element i , F_i^a			Recovery Rate of Element i , R_i (pct) ^b		
	Pt	Pd	Rh	Pt	Pd	Rh
D_150629-16	3.2	3.1	3.2	100 ^c	96	100 ^c
E_151024-18	4.7	4.6	4.8	98	98	100 ^c

^a $F_i = C_{\text{mag},i} / C_{\text{cat},i}$.
^b $R_i = 100 \times (C_{\text{mag},i} \times w_{\text{mag}}) / ((C_{\text{mag},i} \times w_{\text{mag}}) + (C_{\text{nmag},i} \times w_{\text{nmag}}))$.
^c $C_{\text{nmag},i}$ was less than the detection limit of ICP-AES.

However, their magnitudes can be potentially improved by optimizing the pulverization and magnetic separation procedures.

The results obtained in this study indicate that the physical concentration pretreatment containing the FeCl₂ vapor treatment and magnetic separation stages (Figure 1) is a feasible and effective technique for recovering PGMs directly from the catalyst scrap. The FeCl₂ vapor treatment in the presence of metallic Fe can be used to convert PGMs (Pt, Pd, and Rh) in the catalyst scrap into ferromagnetic Fe-PGM alloys. During the alloying procedure, cordierite and Al₂O₃ species (*i.e.*, major components of spent catalysts) remain unreacted. In contrast, La₂O₃ and CeO₂ species, which are often contained in the catalyst layer of the automobile catalyst, react with FeCl₂ vapor and reduce the amount of supplied FeCl₂ species. However, the reaction products including rare-earth oxychlorides can be theoretically removed from the obtained PGM concentrates as nonmagnetic powders *via* magnetic separation.

V. CONCLUSIONS

In this study, a novel method for PGM extraction involving a pretreatment with FeCl₂ vapor was demonstrated. The reactions of typical components of automobile catalysts (including PGMs, cordierite, Al₂O₃, CeO₂, La₂O₃, and ZrO₂) with FeCl₂ vapor in the presence of metallic Fe at a temperature of around 1200 K (927 °C) were examined through thermodynamic analyses and experiments. It was found that the FeCl₂ vapor treatment could effectively convert PGMs (Pt, Pd, and Rh) into ferromagnetic alloys despite the

absence of a physical contact with metallic Fe. Furthermore, cordierite, Al₂O₃, and ZrO₂ did not interact with FeCl₂ vapor, while CeO₂ and La₂O₃ species were converted into their oxychlorides. During the fundamental testing of the samples simulating an automobile catalyst, PGMs were successfully concentrated by magnetic separation after the FeCl₂ vapor treatment. Thus, it can be concluded that the proposed method is a feasible and useful technique for recovering PGMs directly from spent catalysts.

Although further studies are required for its practical implementation, the physical concentration process involving the FeCl₂ vapor treatment can potentially increase the efficiency and throughput of the existing recycling processes when used during the pretreatment stage. Furthermore, because the proposed method does not require a large-scale plant, it can be performed at the collecting and scrapping sites for old automobiles. The automobile catalyst scraps collected at such sites are often transported to smelters by sea or by ground. However, if PGMs are concentrated directly at the collecting and scrapping sites, they can be transported by air to refineries for further treatment. Using this new recycling route, PGMs can be potentially recovered within a relatively short lead time.

ACKNOWLEDGMENTS

The authors are grateful to Dr. Katsuhiro Nose (The University of Tokyo, currently with JX Nippon Mining & Metals Corporation), Mr. Tetsuo Watanabe (The University of Tokyo, currently with Tanaka

Kikinzoku Kogyo K. K.), Dr. Takanari Ouchi, Mr. Ryohei Yagi, Mr. Akihiro Iizuka (The University of Tokyo) for their valuable suggestions and comments. The authors thank Marusu Glaze Co., Ltd. for providing cordierite powder. This research was financially supported by the Japan Society for the Promotion of Science (JSPS) through the Grant-in-Aid for Scientific Research (S) (KAKENHI Grant No. 26220910) and by the Mazda Foundation.

REFERENCES

1. PGM Market Report May 2017 Summary of Platinum Supply and Demand in 2016 (Johnson Matthey Plc., 2017), <http://www.platinum.matthey.com/services/market-research/pgm-market-reports>. Accessed 5 Dec 2017.
2. F. Habashi (ed.): *Handbook of Extractive Metallurgy*, VCH Verlagsgesellschaft mbH, Weinheim, 1997, vol. III, pp. 1269–26.
3. F.K. Crundwell, M.S. Moats, V. Ramachandran, T.G. Robinson, and W.G. Davenport: *Extractive Metallurgy of Nickel, Cobalt and Platinum-Group Metals*, Elsevier, Oxford, 2011.
4. S. Seetharaman (ed.): *Treatise on Process Metallurgy, Volume 3: Industrial Processes*, Elsevier, London, 2013, pp. 1071–97.
5. R.K. Mishra: *Proceedings of the 17th International Precious Metals Conference*, 1993, pp. 449–74.
6. S. Suzuki, M. Ogino, and T. Matsumoto: *J. MMIJ.*, 2007, vol. 123, pp. 734–36 (in Japanese).
7. M. Benson, C.R. Bennett, J.E. Harry, M.K. Patel, and M. Cross: *Resour. Conserv. Recycl.*, 2000, vol. 31, pp. 1–7.
8. H. Dong, J. Zhao, J. Chen, Y. Wu, and B. Li: *Int. J. Miner. Process.*, 2015, vol. 145, pp. 108–13.
9. F.L. Bernardis, R.A. Grant, and D.C. Sherrington: *React. Funct. Polym.*, 2005, vol. 65, pp. 205–17.
10. S. Owada, H. Seshimo, M. Miyashita, and K. Fujiwara: *Proceedings of the 2nd International Symposium on East Asian Resources Recycling Technology*, 1993, pp. 69–77.
11. S. Owada, Y. Tsubuku, and H. Nakayama: *Proceedings of MMIJ Spring Meeting*, 1994, pp. 282–83 (in Japanese).
12. S. Owada and K. Shinoda: *Proceedings of MMIJ Spring Meeting*, 2006, pp. 69–70 (in Japanese).
13. W. Kim, B. Kim, D. Choi, T. Oki, and S. Kim: *J. Hazard. Mater.*, 2010, vol. 183, pp. 29–34.
14. G. Liu, T. Ichinose, A. Tokumaru, and S. Owada: *Mater. Trans.*, 2015, vol. 55, pp. 978–85.
15. G. Liu, A. Tokumaru, and S. Owada: *Resour. Process.*, 2013, vol. 60, pp. 28–35.
16. T.H. Okabe and J. Mitsui: Japan Patent, P5946034, 2016 (in Japanese).
17. Y. Taninouchi, T. Watanabe, and T.H. Okabe: *Mater. Trans.*, 2017, vol. 58, pp. 410–19.
18. Y. Taninouchi, T. Watanabe, and T.H. Okabe: *Metall. Mater. Trans. B.*, 2017, vol. 48B, pp. 2027–36.
19. Y. Taninouchi and T.H. Okabe: in *Rare Metal Technology 2017 (Proceedings of the TMS 2017 Annual Meeting and Exhibition (TMS2017))*, Springer, Cham, 2017, pp. 119–27.
20. Y. Taninouchi and T.H. Okabe: *Mater. Trans.*, 2018, vol. 59, pp. 88–97.
21. Y. Danzaki and T. Ashino: *Anal. Sci.*, 2001, vol. 17, pp. 1011–113.
22. H. Sasaki and M. Maeda: *J. Phys. Chem. C.*, 2013, vol. 117, pp. 18457–63.
23. I. Barin: *Thermochemical Data of Pure Substance*, 3rd ed., VCH Verlagsgesellschaft mbH, Weinheim, 1995.
24. P. Franke and D. Neuschütz (eds.): *Binary Systems. Part 3: Binary Systems from Cs-K to Mg-Zr*, Springer, Cham, 2005.
25. H. Okamoto (ed.): *Phase Diagrams of Binary Iron Alloys*, ASM International, Ohio, 1993.
26. P. Fredriksson and S. Seetharaman: *Scand. J. Metall.*, 2001, vol. 30, pp. 258–64.
27. D.D. Wagman, W.H. Evans, V.B. Parker, R.H. Schumm, I. Halow, S.M. Bailey, K.L. Churney, and R.L. Nuttall: *J. Phys. Chem. Ref. Data.*, 1982, vol. 11.
28. T.H. Okabe, C. Zheng, and Y. Taninouchi: *Metall. Mater. Trans. B.*, 2018, <https://doi.org/10.1007/s11663-018-1172-4>.